Rotationally Resolved IR-Diode Laser Studies of Ground-State CO_2 Excited by Collisions with Vibrationally Excited Pyridine

Jeremy A. Johnson,[†] Kilyoung Kim, Maurine Mayhew, Deborah G. Mitchell, and Eric T. Sevy*

Department of Chemistry and Biochemistry, Brigham Young University, Provo, Utah 84602

Received: August 14, 2007; In Final Form: January 2, 2008

Relaxation of highly vibrationally excited pyridine (C_5NH_5) by collisions with carbon dioxide has been investigated using diode laser transient absorption spectroscopy. Vibrationally hot pyridine ($E' = 40\,660$ cm^{-1}) was prepared by 248 nm excimer laser excitation followed by rapid radiationless relaxation to the ground electronic state. Pyridine then collides with CO_2, populating the high rotational CO_2 states with large amounts of translational energy. The CO_2 nascent rotational population distribution of the high-J ($J = 58-80$) tail of the 00^00 state was probed at short times following the excimer laser pulse to measure rate constants and probabilities for collisions populating these CO_2 rotational states. Doppler spectroscopy was used to measure the CO_2 recoil velocity distribution for $J = 58-80$ of the 00^00 state. The energy-transfer distribution function, $P(E,E')$, from $E' - E \sim 1300-7000$ cm^{-1} was obtained by re-sorting the state-indexed energy-transfer probabilities as a function of ΔE. $P(E,E')$ is fit to an exponential or biexponential function to determine the average energy transferred in a single collision between pyridine and CO_2. Also obtained are fit parameters that can be compared to previously studied systems (pyrazine, C_6F_6, methylpyrazine, and pyrimidine/CO_2). Although the rotational and translational temperatures that describe pyridine/CO_2 energy transfer are similar to previous systems, the energy-transfer probabilities are much smaller. $P(E,E')$ fit parameters for pyridine/CO_2 and the four previously studied systems are compared to various donor molecular properties. Finally, $P(E,E')$ is analyzed in the context of two models, one indicating that $P(E,E')$ shape is primarily determined by the low-frequency out-of-plane donor vibrational modes, and the other that indicates that $P(E,E')$ shape can be determined from how the donor molecule final density of states changes with ΔE.

I. Introduction

Scientists have long recognized the importance of collisions and energy-transfer processes in understanding the overall kinetics and dynamics of unimolecular processes.[1] As a result, energy transfer has long been an important and fruitful field of study. Of particular importance is an understanding of the fate of complex molecules possessing chemically significant amounts of energy. Key to understanding the overall rate of product formation in unimolecular processes is the energy-transfer probability distribution function, $P(E,E')$, which describes the probability that a molecule initially at energy E', will possess, following a collision, energy E.[2] Despite the importance of this function, and 85 years of interest in energy transfer and its relationship to unimolecular processes, it has only been in the past 10 years that experimental techniques have measured this function.[3−5]

The transient IR laser probe technique, developed by Flynn,[6−10] and currently used by Mullin[11−20] and our lab,[21−23] is capable of studying the relaxation of relatively complex molecules with chemically significant amounts of energy by collisions with spectroscopically tractable bath molecules. The power of this technique lies in the use of high-resolution spectroscopy to study energy gain by simple bath molecules. Lead salt diode lasers (or alternatively F-center lasers) have a frequency bandwidth of $\Delta\nu = 0.0003$ cm^{-1} (0.0001 cm^{-1}), an order of magnitude narrower than the room-temperature width of a rovibrational transition for simple molecules such as CO_2 (0.0042 cm^{-1}). Thus, it is possible to spectroscopically measure not only the number of CO_2 bath molecules scattered into a particular rovibrational state and the rate constant for the energy-transfer process but also the amount of translational recoil using Doppler spectroscopy. In this manner, a detailed picture of the energy-transfer process can be obtained through the eyes of the bath. Studies using this technique have led to a wealth of understanding regarding the dynamic features of both V → V and V → RT energy-transfer processes from aromatic donors, on the verge of unimolecular breakup, to simple bath molecules such as CO_2,[7−14,17−22] H_2O,[15] and more recently DCl.[16]

In addition to the dynamic information obtained in these studies, it is possible to reconstruct the state-resolved data to obtain $P(E,E')$.[3] An understanding of the relationship between molecular properties and $P(E,E')$ is beginning to develop.[10,21,22] Several molecular attributes have been associated with various features of $P(E,E')$, including donor density of states, number of donor molecule vibrational modes, as well as the number of low-frequency modes, and the proximity of the donor molecule to its dissociation threshold. Two models have provided particular insight into understanding the shape and magnitude of $P(E,E')$. The first is an $f(E,E')$ model,[10,21,22] which uses different donor modes to model $P(E,E')$ and determine how well energy transfer resulting from that single vibrational mode mirrors the shape of $P(E,E')$. The second is an application of Fermi's Golden

* Author to whom correspondence should be sent. Electronic mail: esevy@byu.edu. Phone: 801-422-7235. Fax: 801-422-0153.

[†] Present address: Department of Chemistry, Massachusetts Institute of Technology, Cambridge, MA 02139.

10.1021/jp076543d CCC: $40.75
Published on Web 03/06/2008

Rule,[12−15] which has shown a correlation between the shape of $P(E,E')$ and the way the donor density of states changes with ΔE. This work is part of our ongoing efforts to understand what molecular properties affect the shape and magnitude of $P(E,E')$.

Here we present results of the collisional relaxation of highly vibrationally excited pyridine ($E' = 40\ 660\ cm^{-1}$) by collisions with a bath of CO_2. State-resolved data of rotational and translational excitation of CO_2 along with the energy-transfer rate constants and probabilities are re-sorted to obtain $P(E,E')$ for this system, which we then compare to previously studied systems at this internal energy. Particular attention is paid to comparing trends in the shape of $P(E,E')$ with trends in molecular properties, as well as testing the success of these two models at understanding and predicting $P(E,E')$.

II. Experimental Section

The UV pump, IR probe technique used to study the collisional relaxation of highly vibrationally excited pyridine has been described in detail elsewhere;[21] therefore, only a brief outline of the method is presented here. A 1:1 mixture of gas-phase pyridine and CO_2 flows through a 3.0 m Pyrex collision cell at a total pressure of 20 mTorr. A 248 nm KrF excimer laser (Lamda Physik Complex 201) is used to excite the $S_2 \leftarrow S_0$ transition of pyridine.[24,25] Pyridine UV absorption increases linearly with laser intensity up to 23 mJ/cm^2; energy-transfer studies were performed at several laser intensities between 5 and 20 mJ/cm^2 to ensure that the energy-transfer results were independent of laser intensity. These intensities resulted in a typical fraction of excited pyridine molecules between 7×10^{-3} and 2×10^{-2}. Electronically excited pyridine then undergoes rapid radiationless internal conversion (<1 ps) into highly vibrationally excited states of the ground electronic state with a nearly unity quantum yield.[24] Energy gain into individual rotational states of the CO_2 (00^00) vibrational state resulting from collisions with vibrationally hot ground electronic state pyridine is monitored by probing the transient absorption of IR light ($\lambda = 4.3\ \mu m$) that is collinearly propagated with the UV beam through the collision cell. The highly resolved (0.0003 cm^{-1}) IR laser (Laser Components) is used to probe the scattered CO_2 molecules via the antisymmetric stretch transition of CO_2. To ensure that only a single diode laser mode is detected, the infrared light is passed through a single grating monochromator (Acton Spectra pro 500i) before being focused onto a liquid nitrogen cooled InSb detector (Judson Technologies). The detector and pre-amplifier (Perry Amplifier) combination has a rise time of approximately 400 ns, shorter than one-fourth the gas kinetic collision time (1 μs). The signal from the InSb detector is digitized and stored on a LeCroy LT342 Waverunner digital oscilloscope before being transferred to a computer for further analysis. Approximately four percent of the infrared light is split off and passed through a reference line. The reference beam passes through a monochromator and is focused onto a high-gain InSb detector (Judson Technologies); the output of the reference detector is used as input to a lock-in amplifier (Stanford Research Systems). The lock-in amplifier generates an error signal that is fed back to the diode laser control electronics allowing active stabilization of the laser frequency.

Determination of rovibrational-state populations requires a measurement of both the transient absorption at the center of the line and the Doppler broadened line shape; therefore, two types of measurements are collected for each rotational state: the transient fractional absorption, $\Delta I/I$, after 1 μs (one-fourth the gas kinetic collision time of 4 μs) and the Doppler-broadened full width at half maximum (fwhm). The center line measurement is obtained by locking the diode laser frequency to the appropriate CO_2 line and averaging the absorption over approximately 100 excimer laser shots. A dual channel technique[8] is employed to account for short-term fluctuations in the diode laser intensity, and a reference line scheme[26] is used with the center line measurements to correct for longer term drifts in the system. Additional short-cell and long-cell reference procedures[21] are performed to determine the absolute scattering rate constant and to calibrate the measured probabilities to previously measured systems. Line shape measurements are performed by locking the diode laser frequency to the peak of a scanning Fabry−Perot Etalon fringe (free spectral range = 289 MHz). Absorption by CO_2 is then measured at a series of 30−40 frequencies distributed evenly over the line shape, averaged over 100 excimer laser shots at each frequency.

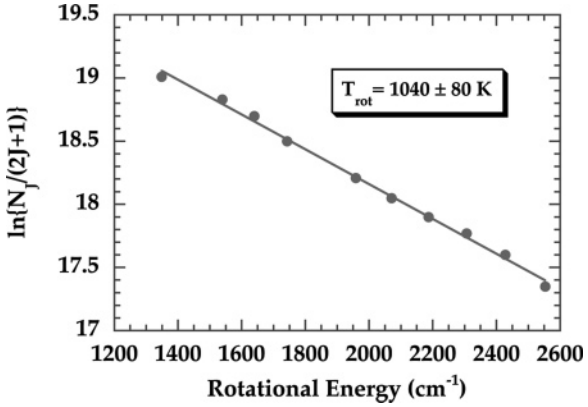

Figure 1. Boltzmann plot of the nascent rotational distributions in the ground vibrational level of CO_2 following excitation by collisions with vibrationally hot pyridine. The solid line is the best linear least-squares fit to the experimental points measured over the range $J = 58-80$. The slope of the best fit line is equal to $-1/kT_{rot}$ and the number densities, $N(J)$, are in units of molecules/cm^3. The rotational temperature for CO_2 molecules scattered into the high-J states is 1040 ± 80 K.

Pyridine (Aldrich, HPLC grade) and pyrazine (Aldrich, 99+%) were purified prior to experiments using no fewer than three freeze (77 K)−pump−thaw cycles, and research-grade CO_2 (Intermountain Airgas Inc., 99.999%) was used without further purification.

III. Results

A. Rotational and Translational Excitation of the Carbon Dioxide Bath. Transient CO_2 populations in various J states of the ground vibrational level, ranging from $J = 58-80$, were monitored via infrared absorption following UV excitation of pyridine at 248 nm. Because the CO_2 rotational[27−32] and translational[33] energies change with each collision, the distributions probed at short times after the excimer laser pulse represent the nascent collision dynamics without significant relaxation. Results for these studies are consistent with similar studies on other systems in that significant excitation of the high CO_2 rotational states indicates a large degree of rotational excitation. A Boltzmann plot of the rotational distribution created by collisions of CO_2 with hot pyridine (Figure 1) indicates that rotational distribution over this range of final J states is described by a single rotational temperature. The measured rotational temperature of 1040 ± 80 K, within the range of rotational temperatures reported for previously studied systems, indicates that collisions with pyridine scatter CO_2 molecules into high-J states transferring large amounts of rotational energy in a single collision.

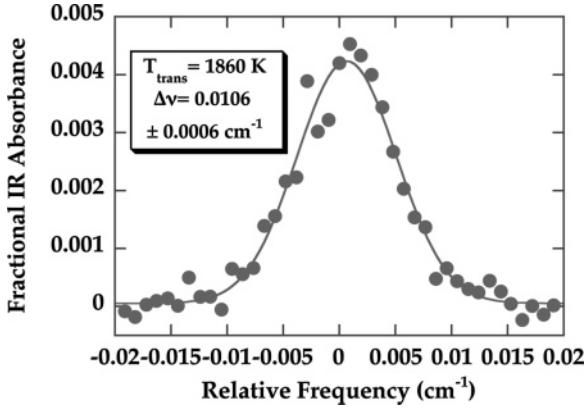

Figure 2. Nascent Doppler broadened line shape for the absorption transition CO_2 (00^00;J=70) → CO_2 (00^01;J=69) probing CO_2 molecules excited by collisions with vibrationally excited pyridine. The line shape was obtained using a flowing mixture of 10 mTorr pyridine and 10 mTorr CO_2. The points represent the fractional IR absorption of CO_2 collisionally scattered in the 00^00, $J = 70$ state measured 1 μs following 248 nm excimer laser pumping of pyridine. Absorption measurements are averaged over approximately 100 excimer laser shots fired at 1 Hz at each frequency across the line. The solid line is the best nonlinear least-squares fit to a Gaussian function. The line width obtained from this fit is 0.0106 ± 0.0006 cm^{-1}. For comparison, the fwhm of a CO_2 line shape with $T_{trans} = 300$ K is approximately 0.0042 cm^{-1}.

The projection of lab frame CO_2 recoil velocities onto the laser probe axis was determined from measurements of the Doppler broadened lineshapes of the final CO_2 rotational states. As seen in Figure 2, a Gaussian function accurately fits the measured lineshapes, indicating that a single translational temperature can suitably describe the CO_2 translational excitation. Figure 2 shows the transient absorption line shape obtained from a measurement taken at 1 μs after excimer laser excitation of a mixture of 10 mTorr of pyridine and 10 mTorr of CO_2. The line width (fwhm) obtained from probing CO_2 scattered into $J = 70$ is $\Delta\nu = 0.0106 \pm 0.0006$ cm^{-1}, corresponding to a lab frame temperature of 1860 K. For comparison purposes, the line width of a transition probing CO_2 molecules with a room-temperature velocity distribution is $\Delta\nu = 0.0042$ cm^{-1}. Previous studies[8] indicate that the post-collision velocity distributions are isotropic; thus, measured translational temperatures describe the three-dimensional speed distribution of the CO_2 molecules following collisions with highly vibrationally excited pyridine.

Full-width, half-maximum Doppler line widths for the absorption transitions probing scattering into J states between 58 and 80 are given in Table 1, along with the corresponding lab frame translational temperatures, and the pyridine/CO_2 *relative* (center of mass) translational temperatures, which are more relevant for determining the actual energy transfer in these collisions. As can be seen in the data in Table 1, collisions scattering CO_2 molecules into high angular momentum states produce broad (high-temperature) velocity distributions, suggesting that these collisions are accompanied by large translational energy transfers. CO_2 line widths also vary nearly linearly with the final rotational angular momentum as was observed in other systems.[7,8,10,21,22] This near linear relationship, illustrated graphically in Figure 3, is an indication of a constant pyridine/CO_2 effective impact parameter.[7,10]

B. Final State-Resolved Energy-Transfer Rate Constants and Probabilities. The state specific rate constant, k_2^J, for excitation of CO_2 from a thermal distribution into state J at

TABLE 1: Full Width at Half-Maximum Doppler Line Widths,[a] Translational Temperatures,[b] and Center of Mass Translational Temperatures[c] for the Process Pyridine$^{E'}$ + $CO_2(00^00)$ → Pyridine^{E} + $CO_2(00^00,J,V)$[d]

final CO_2 rotational level J	$\Delta\nu_{obs}$, cm^{-1} [a]	T_{trans}, K[b]	T_{com}, K[c]
58	0.0079 ± 0.0004	1012 ± 115	1410 ± 180
64	0.0106 ± 0.0007	1840 ± 240	2710 ± 380
66	0.0086 ± 0.0007	1230 ± 200	1750 ± 310
70	0.0099 ± 0.0007	1620 ± 220	2360 ± 350
72	0.0106 ± 0.0006	1860 ± 210	2730 ± 280
74	0.0110 ± 0.0007	2000 ± 250	3950 ± 390
76	0.0116 ± 0.0007	2240 ± 275	3330 ± 430
78	0.0114 ± 0.0007	2180 ± 260	3220 ± 410
80	0.0131 ± 0.0012	2870 ± 520	4300 ± 800

[a] The measured full width at half-maximum of the transient Doppler line widths for the transitions $CO_2(00^00,J) \rightarrow CO_2(00^01,J-1)$, determined 1 μs after pyridine excitation in a 1:1 sample of pyridine:CO_2 at a total pressure of 20 mTorr. The thermal Doppler line width for CO_2 at $T = 298$ K is $\Delta\nu_0 = 0.0042$ cm^{-1}. [b] The final translational temperature, T_{trans}, is obtained from fitting the experimentally determined Doppler lineshapes to a Gaussian function, and it is related to the line width, $\Delta\nu_{obs}$ (full width half-maximum) through the expression $T_{trans}(K) = mc^2(\Delta\nu_{obs})^2/(8R \ln 2(\nu_0)^2)$, where m is the mass of CO_2, c is the speed of light, R is the gas constant, and ν_0 is the wavenumber at the center of the absorption line. [c] The final center of mass translational temperature, T_{com}, is obtained from the expression $T_{com}(K) = T_{trans} + (T_{trans} - T)(m_{CO_2}/m_{pyridine})$, where T_{trans} is the temperature describing the CO_2 lab frame velocity, T is the ambient cell temperature, and m is the mass of CO_2 and pyridine, respectively. [d] The internal energy of pyridinefollowing 248 nm excitation is $E' = 40\,660$ cm^{-1}.

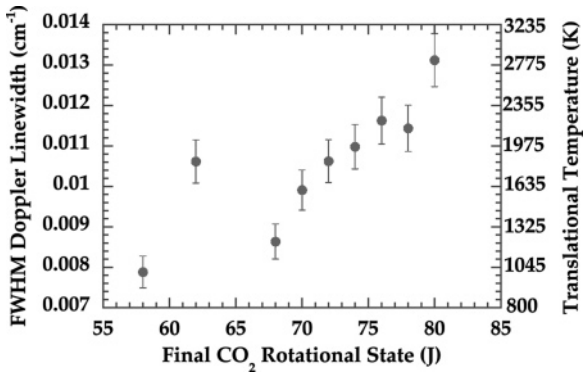

Figure 3. The fwhm Doppler line width of absorption transitions probing high rotational states of CO_2 following excitation by collisions with vibrationally hot pyridine ($E' = 40\,660$ cm^{-1}) is plotted against the final rotational state J. The lab frame translational temperatures, which are determined from the measured line widths, are given on the right y-axis. The line widths are measured 1 μs following 248 nm excimer laser excitation of the pyridine, ensuring that the measured velocity distributions are nascent ($\tau_{coll} \approx 4$ μs). The fwhm appropriate for a 298 K velocity distribution is 0.0042 cm^{-1}. The line width for $J = 62$ appears to be an outlier from remainder of the results.

times much less than the mean gas kinetic collision time can be obtained from the expression

$$k_2^J = \frac{[CO_2(00^00,J,V)]}{[CO_2]_0[\text{pyridine}^{E'}]_0\, t} \qquad (1)$$

$[CO_2]_0$ is the bulk carbon dioxide number density, $[\text{pyridine}^{E'}]_0$ is the number density of pyridine molecules excited by the excimer laser pulse to an energy E', determined from the UV absorption, and $[CO_2(00^00,J,V)]$ is the state specific CO_2 concentration, obtained from infrared absorption measurements.

The absolute rate constants for the excitation of CO_2 into the high-J tail of the (00^00) vibrational state by collisions with

TABLE 2: Rate Constants[a] (k_2^J) and Probabilities[b] (k_2^J/k_{LJ}) for the Energy-Transfer Process Pyridine$^{E'}$ + $CO_2(00^00)$ → Pyridine^E + $CO_2(00^00,J,V)$

final CO_2 rotational level J	$10^{12}k_2^J$	10^3 $Prob_{LJ}$
58	2.3 ± 0.6	3.6 ± 0.9
64	2.0 ± 0.5	3.1 ± 0.8
66	1.6 ± 0.4	2.5 ± 0.6
70	1.3 ± 0.3	2.0 ± 0.5
72	1.2 ± 0.3	1.8 ± 0.5
74	1.0 ± 0.3	1.6 ± 0.4
76	0.8 ± 0.2	1.2 ± 0.3
78	0.6 ± 0.1	0.2 ± 0.2
80	0.6 ± 0.1	0.3 ± 0.2

[a] All rate constants are given in units of cm^3 $molecule^{-1}$ s^{-1}. [b] The probability for energy transfer is given as $Prob_{LJ} = k_2^J/k_{LJ}$, where k_{LJ} is the Lennard-Jones kinetic collision rate constant. It is defined (see ref 43) as $k_{LJ} = \pi[(d_{CO_2} + d_{pyridine})/2]^2[(8k_BT)/(\pi\mu)]^{1/2}\Omega_{12}$, where d_{CO_2}= 4.5 Å, ref 44, $d_{pyridine}$ = 5.27 Å (assumed to be equal to that for benzene, ref 44), k_B is Boltzmann's constant, and μ is the reduced mass. Ω_{12} is the Lennard-Jones collision integral given by the following expression:[36] $\Omega_{12} = [0.636 + 0.567 \log(kT/\epsilon_{12})]^{-1}$, where ϵ_{12} is the pyridine−CO_2 well depth with ϵ_{CO_2}/k = 195 K, ref 44, $\epsilon_{pyridine}/k$ = 445.21 K, ref 45, and $\epsilon_{12} = [\epsilon_{CO_2}\epsilon_{pyridine}]^{1/2}$. The Lennard-Jones collision rate constant for pyridine/CO_2 at 298 K is 6.45 × 10^{-10} cm^3 $molecule^{-1}$ s^{-1}.

hot pyridine (E' = 40 660 cm^{-1}) are given in Table 2. These rate constants are scaled both on an absolute scale and to previous pyrazine/CO_2 scattering studies[8] such that data can be directly and accurately compared to other studies at 248 nm. Table 2 also includes the Lennard-Jones scattering probabilities for excitation of each final rotational state. The probability that a CO_2 molecule is scattered into a particular final J state is defined as the energy-transfer rate constant, k_2^J, divided by the Lennard-Jones collision rate constant,

$$\text{Prob}^J = \frac{k_2^J}{k_{LJ}} \tag{2}$$

The choice of the Lennard-Jones has been discussed elsewhere[21] and is used for consistency in comparing results system to system, even though it has been shown to be in error by as much as a factor of 2 for systems similar to those studied here.[34]

C. Energy-Transfer Probability Distribution Function. The energy-transfer probability distribution function, $P(E,E')$, for the large ΔE region can be obtained from state-resolved data reported here using a conversion process detailed elsewhere.[3] Because the conversion of quantum-state-resolved probabilities to ΔE-indexed probabilities requires both the CO_2 final states (well defined in these experiments) and CO_2 initial states (defined only by the initial temperature distribution), detailed temperature-dependent measurements of the energy-transfer process along with an energy-transfer gap law model were used to provide the average initial rotational state for previously studied systems.[8−10] In previously studied cases, the average initial J state was found to be 28.7 ± 3. Because the difference in rotational energy between the initial and final states for a linear molecule goes as the difference in J^2, uncertainty in the final state produces a greater error than does uncertainty in the initial state. Using 28.7 as the average initial rotational state for previous temperature-dependent studies would result in a error of 2.2 and 5.1% for J_f = 82 and 58, respectively. Because this error is about the same as or smaller than other experimental errors associated with this experiment, temperature-dependent studies have not been performed for the pyridine/CO_2 system and we have used 28.7 as the average initial rotational state to calculate $P(E,E')$. Unlike the average initial J, temperature-dependent studies are not necessary to determine the average initial relative velocity; these have been calculated, as before, using a translational gap law model.[8]

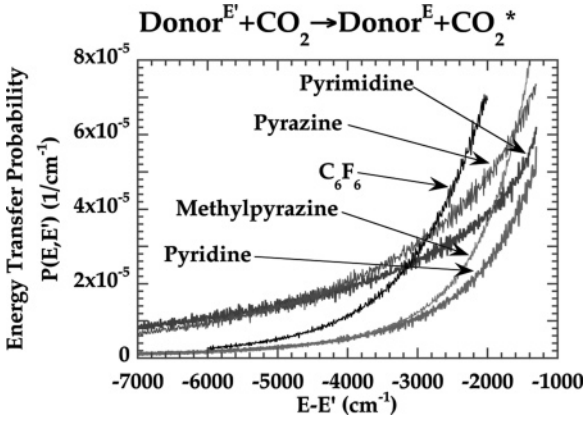

Figure 4. Plots of the high ΔE tail of the energy-transfer probability distribution function describing the first Lennard-Jones collision between a vibrationally excited donor molecule (pyridine, pyrimidine,[21] pyrazine,[8] C_6F_6,[9] or methylpyrazine[10]) at energy $E' \approx$ 41 000 cm^{-1} and a CO_2 bath molecule resulting in CO_2 excitation into high rotational angular momentum states (J = 58−82) of the ground vibrational level. E is the energy of the hot donor molecule following the collision.

The energy-transfer distribution function for single collisions between pyridine and carbon dioxide is plotted in Figure 4. (Note that the probability is plotted against $E-E'$ where E' = 40 660 cm^{-1} and E is the final donor energy.) Comparing the energy-transfer distribution function obtained from the J = 58−80 data to one obtained from data extrapolated over the full range of CO_2 rotational states indicates that $P(E,E')$ in the energy range ΔE > 1300 (shown in Figure 4) is well determined in these experiments (see ref 3). A primary aspect of this work is to determine how molecular properties affect the energy-transfer probability distribution function; therefore, $P(E,E')$ for the pyridine/CO_2 system is compared to $P(E,E')$ obtained from similar studies of pyrazine,[3,8] hexafluorobenzene,[3,9] methylpyrazine,[10] and pyrimidine[21] excited to the same energy and relaxed by CO_2. To facilitate comparison, Figure 4 also contains $P(E,E')$ for these previously studied species. For all donor molecules, single collisions with $\Delta E \geq$ 2000 cm^{-1} are clearly evident; however, this "supercollision" tail behaves differently for each molecule. Because $P(E,E')$ is a normalized function, curves for different molecules must either cross each other or be identical over the entire ΔE range. This requires that any comparison between $P(E,E')$ for different systems specify both final and initial energy to be meaningful. As a result, it is convenient to fit the measured $P(E,E')$s to a model function, such that one or two values can be used for comparison.

The energy-transfer distribution functions shown in Figure 4 have been fit to both a single and a biexponential functional form. As also seen in previously studied systems,[3,9,10,21] single-exponential fitting of $P(E,E')$ provides a poor fit to the experimentally obtained distribution function, when normalization and detailed balance are considered; however, the biexponential model accurately fits the data with those restrictions. The normalized, biexponential model, which has been used to include both strong and weak collisions, is given for down collisions according to[35]

$$P(E,E') = \frac{(1-f)\exp\{-(E'-E)/\alpha\} + f\exp\{-(E'-E)/\gamma\}}{(1-f)(\alpha+\beta) + f(\gamma+\delta)} \qquad E \leq E' \tag{3}$$

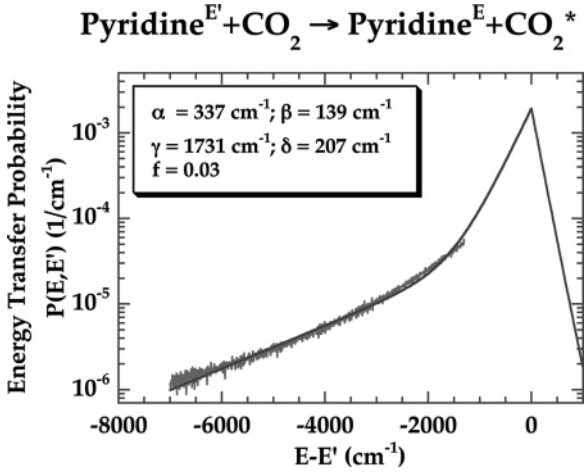

Figure 5. Plot (noisy line) of the energy-transfer distribution function for the pyridine/CO_2 system with $E' = 40\,660$ cm^{-1} along with the best-fit biexponential model function (eq 3) (solid line). The best fit parameters (α, β, γ, δ, and f) are defined in the text following eq 3. E is the energy of the hot donor molecule following the collision. The $P(E,E')$ shown is calculated on the basis of the estimated values of $J_i = \langle J \rangle = 28.7$ for the mean initial rotational state, J_i, for collisions populating high-J_f states ($J_f \approx 58-80$) of CO_2.

In this model α is the average energy transfer for downward "weak" collisions, and γ is the average energy transfer for downward "strong" ("super") collisions. The up collision side of the model function is similar with differences being the exchange of E and E' and the substitution of α and γ with β and δ, the respective average energy transfers for the upward "weak" and "strong" collisions. The up collisions parameters are related to the down collision parameters by detailed balance.[36] The separation into strong and weak collisions is somewhat arbitrary; however, the biexponential model is used in systems where the large ΔE tail of $P(E,E')$ has a greater probability than can be fit with a single-exponential function. Because both the strong and weak-collision channels are peaked at $\Delta E = 0$ cm^{-1}, f cannot be literally interpreted as the fraction of supercollisions, although it is sometimes referred to as this. However, the fraction of large ΔE collisions does get larger with increasing f. The relative importance of supercollisions in $P(E,E')$, however, depends on the magnitude of both f and γ. The energy-transfer probability distribution function along with the best fit, biexponential model function (eq 3) is shown in Figure 5 for the pyridine/CO_2 system.

IV. Discussion

A. Comparison to Pyridine/CO_2 Studies at Lower Internal Energies. Mullin and co-workers have studied the relaxation of vibrationally excited pyridine by CO_2 following excitation at 251, 259, 266, and 271 nm.[11,12] They observed that energy-transfer rate constants, rotational temperatures, and translational temperatures were independent of internal energy over this region. Each of these parameters obtained in the present study are larger than those measured in the Mullin experiments. $T_{rot} = 1040$ vs 850 K (a 20% increase), T_{trans} ($J = 70$) = 1860 vs 1520 K (a 9% increase),and k_2^J is greater by a factor of 3. Although pyridine multiphoton UV absorption in the present study would provide a simple explanation of the observed differences, we have studied the energy transfer at UV intensities ranging from 5 to 20 mJ/cm^2, below the onset of multiphoton absorption at ~23 mJ/cm^2; over this range, T_{rot}, T_{trans}, and k_2^J are independent of laser intensity. Another possible explanation for largest of these differences (k_2^J) could be the way absolute rate constants are determined. Because of excimer beam divergence over the length of the 3 m cell, a short-cell study is necessary to obtain a scaling constant for long-cell measurements. The Nd:YAG pumped Ti:sapphire laser beam used in the Mullin experiments does not suffer from the same degree of divergence as does the excimer; however, a similar scaling procedure is presumably performed in their studies as well. However, this would not explain differences in the rotational and translational temperatures. Additionally, we perform a second experiment to scale our rate constants.[21] This second scaling procedure scales our results to the pyrazine/CO_2 work of Flynn[8] and gives the same scaling factor as the short-cell procedure, within experimental error.

A more interesting possibility for the differences between the Mullin studies and the current work is the onset of a strong-collision channel. Similar onsets have been observed in energy-dependent studies of the pyrazine/CO_2 system.[17−19] Mullin and co-workers observed similar changes to T_{rot}, T_{trans}, and k_2^J between 286 and 281 nm. In those studies, T_{rot}, T_{trans}, and k_2^J increased by 26%, 32%, and a factor of 2, respectively. They attributed this enhancement of energy transfer to vibronic coupling and the presence of a new electronic state. For T_{rot} and T_{trans} the change was a step and the new values remained constant with energy from 281 to 246 nm; however, the rate constant continued to increase essentially linearly with increasing internal energy. This suggests that there may be more than one factor involved, one that creates a change in the rotational and translational distributions and one that enhances the energy-transfer rate constant. An additional factor that has been shown to result in energy-transfer enhancement as a function of energy is the proximity to dissociation. In classical trajectory calculations of collisional relaxation of SO_2 by Ar, Lendvay, Schatz, and Harding[37] observed that $\langle \Delta E \rangle$ initially increased linearly with internal energy; however, as SO_2 approached the threshold for dissociation the dependence of energy transfer on internal energy became even stronger than quadratic.

Although there is no new electronic state between 251 and 248 nm in pyridine, there does appear to be some factor that results in the onset of a strong-collision channel. The rate of pyridine internal conversion[24] has been shown to increase in this energy region; however, the increase in internal conversion rate is not nearly as dramatic as the increase in going from the $S_1 \leftarrow S_0$ transition region to the $S_2 \leftarrow S_0$ region (36 000−38 000 cm^{-1}, 277−263 nm). It is interesting to note that Mullin and co-workers did not observe an enhancement in the 270 nm range. Energy-transfer studies at higher energy than 248 nm and lower than 271 nm are necessary to understand the increases observed here. In addition, energy-dependent studies of pyridine dissociation are also necessary to determine the threshold for unimolecular dissociation, which is between 248 and 193 nm,[38] and evaluate the affect of dissociation on pyridine energy transfer in this energy range.

B. Comparison to Other Donor/CO_2 Systems at 248 nm. Collisions with vibrationally hot pyridine that scatter CO_2 into the high rotational states of the ground vibrational level have many of the same features seen in previous studies involving vibrationally hot donor molecules and cold CO_2. The rotational distribution that describes post collision carbon dioxide is characterized by a temperature of 1040 K, which places pyridine in the middle of other donor molecules studied at this internal energy (methylpyrazine,[10] 725 K; C_6F_6,[9] 795 K; pyrazine,[8] 1300 K; pyrimidine,[21] 1680 K). Even though there is no *a priori* reason to suppose that a temperature will describe any part of the rotational distribution created by collisions with vibrationally

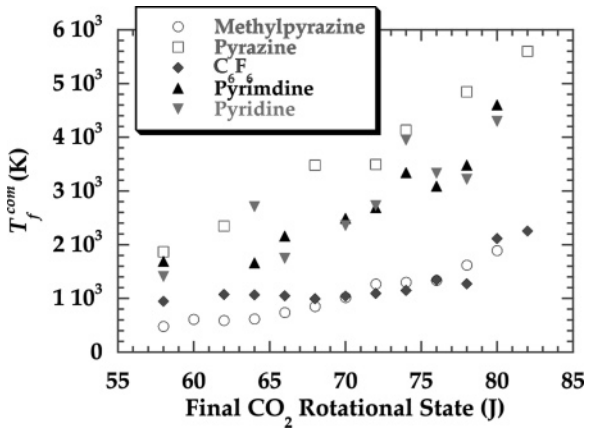

Figure 6. CO_2 *relative* (center of mass) translational temperatures describing translational energy gain by CO_2 in collision with vibrationally excited pyridine, pyrimidine,[21] methylpyrazine,[10] C_6F_6,[9] and pyrazine[8] as a function of final CO_2 rotational state. T_f^{com} describing pyridine/CO_2 collisions is similar to the temperature describing pyrimidine/CO_2 collisions. The slope of T_f^{com} as a function of final CO_2 rotational state is similar for pyrazine, pyrimidine, and pyridine, indicating that the effective impact parameter for each of the donors in collisions with CO_2 is similar.

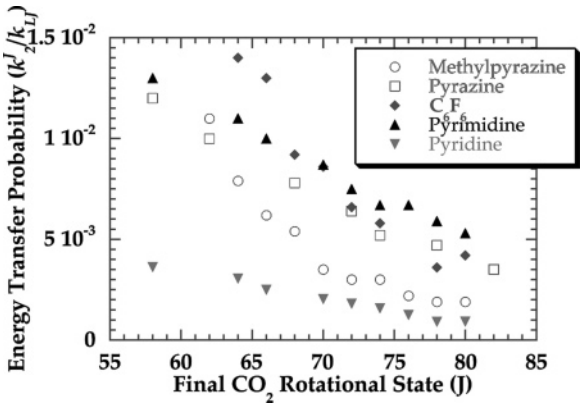

Figure 7. Energy-transfer probability of the first Lennard-Jones collision, $Prob_{LJ} = k_2^J/k_{LJ}$, between vibrationally excited donor molecules (pyridine, pyrimidine, methylpyrazine, C_6F_6, and pyrazine) and CO_2 as a function of final CO_2 rotational state. Note that over the entire range of final *J* states, collisions between vibrationally excited pyridine and CO_2 have the lowest probability of populating the high CO_2 *J* states. For other systems studied, energy-transfer probabilities in this range of ΔE cross one another, as can also be seen in Figure 4, when probability is re-sorted as a function of ΔE.

hot molecules, because a single temperature does characterize these high-*J* states of CO_2 (00^00), it can be viewed as a convenient measure of the amount of rotational excitation. Note that the indicated rotational temperatures only describe the high-*J* tail ($J = 58-80$) of the rotational distribution, and may be very different from any temperature that describes lower rotational states.[10] In fact, for the systems studied thus far at $E' \sim 41\,000$ cm^{-1}, the rotational distribution must be described by at least two different temperatures for $P(E,E')$ to be normalized.

In addition to significant rotational excitation, CO_2 is excited translationally by collisions with pyridine, as indicated by the broad lineshapes of various high-*J* states probed in this study. A comparison of the center of mass temperature data from Table 1 to similar data for previously studied systems, shown in Figure 6, indicates that pyridine imparts a similar amount of translational energy to CO_2 in collisions as pyrimidine, but less than pyrazine and more than methylpyrazine or C_6F_6. As stated above, the linear relationship between translational excitation (as determined by $\Delta\nu$) and final rotational state indicates that the pyridine/CO_2 effective impact parameter is constant for CO_2 excitation over this range of final CO_2 rotation states.[7,10] As seen in Figure 6, not only is the center of mass temperature for pyridine/CO_2 linear with the final *J* state but also the slope is similar to that for pyrazine and pyrimidine, suggesting that these three systems have similar effective impact parameters, not surprising given the similarities between these three molecules in structure and mass.

Although scattering of CO_2 into high-*J* levels following collisions with vibrationally excited pyridine has been observed in these studies with similar rotational and translational temperatures as other systems, the associated energy-transfer probability for pyridine/CO_2 is significantly less than previously studied systems. Figure 7 shows the probability of populating the high-*J* states of CO_2 following collisions with various vibrationally excited donor molecules. For all CO_2 rotational states probed in this study, the probability for scattering is smallest when the collision partner is pyridine, although pyridine and methylpyrazine have similar probabilities for scattering into the highest-*J* states probed. The small energy-transfer probabilities for pyridine/CO_2 scattering are further highlighted by the difference in integrated probability, $Prob_{LJ}^{INT}$, for collisional excitation of the CO_2 high-*J* tail. For pyridine/CO_2 collisions, the integrated probability, determined by the sum of the energy-transfer probabilities ($Prob_{LJ}$) from $J = 58-80$, is $Prob_{LJ}^{INT} = 0.0259$, and $Prob_{LJ}^{INT} = 0.0387$, 0.0902, 0.128, and 0.108 for methylpyrazine,[10] pyrazine,[8] C_6F_6,[9] and pyrimidine,[21] respectively. Because the total energy-transfer probability is normalized, other energy-transfer events, including V−V processes and scattering into the low-*J* states of the ground vibrational level, must be more probable in the pyridine/CO_2 system than other systems.

Mullin and co-workers[11] have studied excitation of both vibrationally ground and excited CO_2 by collisions with pyridine following 266 nm excitation. They found that excitation of the high-*J* tail of ground state CO_2 was 7.7 times more frequent than excitation of the 00^01 vibrationally excited state. A comparison to collisional processes involving vibrationally excited pyrazine at 266 nm indicated that excitation of the high-*J* tail of ground state CO_2 via collisions with vibrationally excited pyrazine was 13 times more probable than excitation of vibrationally excited CO_2. They concluded that the enhancement of CO_2 vibrational excitation in collisions with pyridine was due to the large 2.2 D pyridine dipole moment. The small $Prob_{LJ}^{INT}$ for pyridine/CO_2 relative to other donor/CO_2 systems at 248 nm may be due to enhanced V−V processes or enhanced energy transfer to low *J* of the ground vibrational state; however, because neither of these has been studied, further investigation is necessary to determine definitively the reason for the small $Prob_{LJ}^{INT}$ observed in the pyridine/CO_2 system at 248 nm.

A key aspect of the energy-transfer studies being conducted in our lab involves a desire to understand how the shape and magnitude of the energy-transfer probability distribution function, $P(E,E')$, is related to molecular properties of the molecule involved in the collisional relaxation process. Energy-transfer studies at $E' \sim 41\,000$ cm^{-1} of pyrazine, C_6F_6, methylpyrazine, and pyrimidine with carbon dioxide suggested that the strong-collision energy-transfer magnitude was related to the donor proximity to threshold for unimolecular dissociation, and the fraction of strong collisions (or supercollisions) was related to the number of donor molecule vibrational modes with $\nu < 500$ cm^{-1}.[21] Table 3 lists parameters for exponential and biexponential fits to the experimentally obtained $P(E,E')$, along with

TABLE 3: Energy-Transfer Probability Distribution Function Double Exponential Fit Parameters (Characteristic Energy-Transfer Frequencies for Both Strong and Weak Down Collisions, Fraction of Strong Collisions, and Average Down Collision Energy) as Well as the Total Number of Donor Vibrational Modes, Number of Low-Frequency Vibrational Modes, Precollision Density of States, and Photodissociation Lifetime

	γ^a (cm^{-1})	$\langle\Delta E\rangle_d{}^b$ (cm^{-1})	α^c (cm^{-1})	f^d	s^e	$\rho(E')^f$	$\tau_{dis}{}^g$ (μs)	$s < 500$ cm^{-1} ^{h}
C_6F_6[3]	1411	809	620	0.15	30	2.1×10^{23}		13
methylpyrazine[10]	1527	682	441	0.05	33	8.4×10^{17}	~16	4
pyrazine[3]	2532	536	296	0.05	24	3.9×10^{13}	~6	2
pyrimidine[21]	3342	576	292	0.03	24	1.8×10^{13}	~1	2
pyridine	1731	529	337	0.03	27	2.0×10^{14}		2

[a] The characteristic strong energy-transfer magnitude as determined from the biexponential fit of the $P(E,E')$ data. [b] The average energy transferred in a single downward collision involving vibrationally excited donor and CO_2. Determined using the exponential fit parameters obtained from an exponential fit of the $P(E,E')$ data for each system. [c] The characteristic weak energy-transfer magnitude as determined from the biexponential fit of the $P(E,E')$ data. [d] The fraction of strong collisions as determined from the biexponential fit of the $P(E,E')$ data. [e] The total number vibrational normal modes for the donor molecule. [f] The vibrational density of states for the donor molecule at the energy following the absorption of a 248 nm photon calculated using a Whitten−Rabinovitch algorithm.[46] [g] The photodissociative lifetime of the donor molecule after 248 nm absorption. Lifetimes for C_6F_6, methylpyrazine, pyrazine, pyrimidine, and pyridine are obtained from refs 9, 47, 48−50, 51, and 38 respectively. [h] The number of vibrational normal modes with frequency less than 500 cm^{-1}. Normal-mode frequencies for C_6F_6, methylpyrazine, pyrazine, pyrimidine, and pyridine are obtained from refs 52 and 53, 54, 55, 56, and 57−59, respectively.

various donor molecule properties. Increasing strong-collision energy-transfer parameter (γ) generally correlates with decreasing average downward energy transfer, weak-collision energy-transfer parameter (α), "fraction" of strong collisions (f), number of normal modes, density of states, dissociation lifetime, and number of normal modes with $\nu < 500$ cm^{-1}. These particular molecular properties have been examined because results from classical trajectory[37,39,40] and quantum scattering[41] calculations have been interpreted to indicate that low-frequency modes, particularly those with out-of-plane character, are the modes primarily responsible for large single-collision energy-transfer events, and that energy-transfer efficiency increases with donor internal energy, linearly at low energy and stronger than quadratic at energies approaching dissociation threshold. Donor density of states correlates most accurately with the various energy-transfer parameters listed in Table 3. Of course, state density is influenced by the other molecular properties listed.

A Fermi's Golden Rule model[12−15,21,22] has successfully shown the shape of $P(E,E')$ is correlated with the energy-dependent shape of the donor molecule density of states. This model is given according to[15]

$$P(E,E') \propto |V_{if}|^2 \rho(E)\, \rho(E') \qquad (4)$$

where $\rho(E)$ is the density of states at energy E and V_{if} is the matrix element, $\langle i|H|f\rangle$, that couples initial and final states. To test the effectiveness of this model in correlating the shape of $P(E,E')$ with the energy dependence of the donor density of states, we compare the results from this study with the results of several previous energy-transfer studies involving collisional relaxation of highly vibrationally excited donor molecules ($E' \sim 41\,000$) by carbon dioxide. Figure 8 shows a plot of the inverse of the characteristic energy-transfer parameters (the "slope" of $P(E,E')$) obtained by fitting $P(E,E')$ to eq 3 as a function of the slope obtained from plotting $\ln[\rho(E'-\Delta E)]$ vs ΔE[13] for the collisional relaxation of pyrazine,[8] C_6F_6,[9] methylpyrazine,[10] pyrimidine,[21] and pyridine (this study) by CO_2. As can be readily seen, the inverse of both the strong and weak characteristic energy-transfer values is linearly related to the slope of $\ln[\rho(E'-\Delta E)]$ vs ΔE. The results fit remarkably well, especially considering that the weak-collision parameter is obtained by extrapolation of the data. This correlation between density of states and $P(E,E')$ suggests that the energy dependence of the donor density of states is responsible for the shape of $P(E,E')$. Mullin and co-workers have shown that this relationship holds true for the shape of the tail of the distribution for other aromatic donors[12−14] at slightly lower energies, as well as for deactivation by collisions with water.[15]

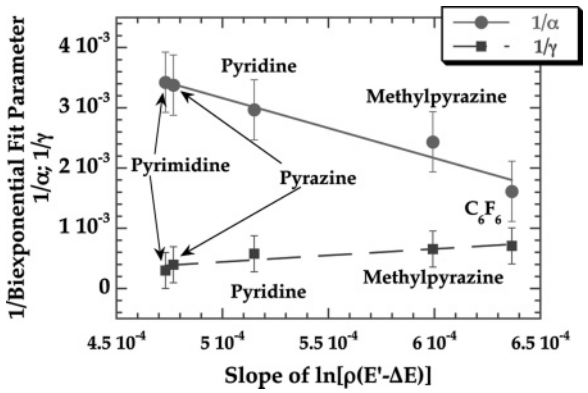

Figure 8. Correlation between the shape of $P(E,E')$ as determined by the biexponential fit parameters ($1/\alpha$ and $1/\gamma$) and the energy-dependent state density of the donor molecules. Squares represent the characteristic energy-transfer magnitude for "strong" collisions (γ), and the circles are the characteristic energy-transfer magnitude for "weak" collisions (α), based on the application of Fermi's Golden Rule to collisional deactivation of vibrationally excited donor molecules in collisions with CO_2. Pyrazine, C_6F_6, methylpyrazine, and pyrimidine data are from refs 3, 9, 10, and 21. The shape of the energy-transfer distribution function as a function of ΔE mirrors the shape of the final donor density of states as a function of energy transferred (ΔE). The shape of both the strong and weak-collision region of $P(E,E')$ is correlated with the donor molecule's final density of states.

There are several interesting aspects about the relationship between the shape of $P(E,E')$ and the energy-dependent shape of the donor density of states, as seen in Figure 8. First, strong-collision energy-transfer magnitude, γ, is smaller for donor molecules whose density of states decrease more rapidly with ΔE. For C_6F_6, the donor with the second most vibrational modes and the most low-frequency modes, the final state density falls off more rapidly than the other donors studied. C_6F_6 also has the smallest value of γ. Pyrimidine and pyrazine, on the other hand, which have the fewest modes and the fewest with low frequency, have the shallowest drop off in density of states with final energy and the largest value of γ. A second interesting feature is that the strong and weak-collision parameters have an opposite correlation with the slope of $\ln[\rho(E'-\Delta E)]$. The strong-collision parameter (γ) becomes smaller as the donor density of states falls off more rapidly with internal energy, and the weak-collision parameter (α) becomes larger with a steeper density of states slope. This may be an indication of a different type of energy-transfer process, one for weak collisions and one for strong collisions. Furthermore, as the slope of $\ln[\rho(E'-\Delta E)]$ becomes steeper (i.e., the decrease in the final donor density of states becomes more precipitous as a function of E) the strong and weak energy-transfer parameters approach each other. In other words, the distinction between weak and strong

TABLE 4: Fractional Vibrational Mode Populations for ν_{16}, a Low-Frequency Out-of-Plane Mode, for Five Donor Molecules (Pyridine, Pyrimidine, Pyrazine, Methylpyrazine, and C_6F_6) at $E' = 41\,000$ cm^{-1} Calculated at Three Different Mode Energies[a]

		$\Delta E = 2000$ cm^{-1}		$\Delta E =$ '4000 cm^{-1}		$\Delta E = 8000$ cm^{-1}	
donor molecule	ν (cm^{-1})[b]	v[c]	f_{v_i}[d]	v[c]	f_{v_i}[d]	v[c]	f_{v_i}[d]
methylpyrazine	ν_{16a} 407	5	0.067	10	0.022	20	0.0021
	ν_{16b} 461	5	0.065	9	0.024	18	0.0021
	ν_{16}[e]		0.132		0.046		0.0042
C_6F_6	ν_{16} 120	17	0.042	34	0.013	67	0.0011
pyrazine	ν_{16a} 340	6	0.058	12	0.024	24	0.0038
	ν_{16b} 416	5	0.068	10	0.028	20	0.0043
	ν_{16}[e]		0.126		0.053		0.0081
pyrimidine	ν_{16a} 347	6	0.058	12	0.024	24	0.0043
	ν_{16b} 398	6	0.068	11	0.029	21	0.0040
	ν_{16}[e]		0.126		0.053		0.0083
pyridine	ν_{16a} 373	6	0.058	11	0.024	22	0.0031
	ν_{16b} 403	5	0.068	10	0.027	20	0.0036
	ν_{16}[e]		0.126		0.051		0.0068

[a] $E' = 41\,000$ is the approximate internal energy of the donors after the absorption of a 248 nm UV photon. [b] Vibrational normal-mode frequencies, ν (cm^{-1}), for C_6F_6, methylpyrazine, pyrazine, pyrimidine, and pyridine are obtained from refs 52 and 53, 54, 55, 56, and 57−59, respectively. [c] Minimum number of quanta for each vibrational mode necessary to effect an energy transfer of at least ΔE. $v = \Delta E/h\nu$. [d] Fraction of donor molecules with v quanta of each vibrational mode at energy $E' = 41\,000$ cm^{-1} calculated according to eq 5. [e] Because ν_{16} is doubly degenerate in C_6F_6, the probability for ν_{16a} and ν_{16b} have been added together for pyridine, pyrimidine, pyrazine, and methylpyrazine to facilitate comparison.

collisions becomes smaller and $P(E,E')$ approaches a single-exponential function. Presumably, at the point where these two curves intersect, $P(E,E')$ changes from biexponential to single-exponential, being described by one energy-transfer parameter. An interesting test case is a system with either more modes or a larger fraction of low-frequency modes, whose state density dependence falls off even more steeply than C_6F_6 that would have a single-exponential $P(E,E')$ at these internal energies.

Although the application of Fermi's Golden Rule here indicates that the donor vibrational frequencies determine the shape of $P(E,E')$, it is not clear if some modes are more important in the energy-transfer process than other modes, and if so, which ones. Clearly, low-frequency modes make the greatest contribution to $P(E,E')$ shape because of their effect on how the donor-state densities depend on internal energy. However, this Fermi's Golden Rule model seems to say that an increased fraction of low-frequency modes, which leads to a steeper change in the energy dependence of the donor density of states, leads to weaker supercollisions, in contradiction to the observations from quantum scattering[41] and trajectory[39,40] results mentioned above. Therefore, despite a clear relationship between shape, donor vibrational mode frequency, and donor density of states, it is not clear how specific donor mode characteristics (frequency and motion) play a role in the shape and magnitude of $P(E,E')$.

Quantum scattering[41] and trajectory[39,40] calculations indicate that the lowest-frequency donor mode is the most efficient at transferring energy. It also indicates that the lower the frequency of a given mode, the more efficient the energy transfer. For ν_{16} the most efficient mode in the benzene/He calculations,[41] this means that C_6F_6 (with $\nu_{16} = 120$ cm^{-1}) is more efficient than pyrazine ($\nu_{16a} = 340$, $\nu_{16b} = 416$ cm^{-1}), methylpyrazine ($\nu_{16a} = 407$, $\nu_{16b} = 461$), pyrimidine ($\nu_{16a} = 347$, $\nu_{16b} = 398$ cm^{-1}), or pyridine ($\nu_{16a} = 373$, $\nu_{16b} = 403$ cm^{-1}); however, efficiency is only half the equation. One must also consider the number of molecules populating a mode with enough energy to impart ΔE. If the population of a given mode at a given energy is small, the magnitude of the energy transfer associated with that energy would be small, regardless of the energy-transfer efficiency of the mode. The fraction of molecules in a given mode at a certain energy can be calculated according to[42]

$$f_{vi} = G_i \frac{\rho_{s-1}(E' - v h\nu_i)}{\rho_s(E')} \tag{5}$$

where $\rho_s(E)$ and $\rho_{s-1}(E' - vh\nu_i)$ are the density of states for all s oscillators at energy E', and the density of states for all oscillators except the mode of interest at an energy of $E' - vh\nu_i$. ν_i is the frequency of the mode of interest, v is the vibrational quantum number of that mode, and G_i is the mode degeneracy. Table 4 tabulates the fraction of molecules in ν_{16} for the five different donor molecules at $E' = 41\,000$, at three different mode energies. Even though ν_{16} in C_6F_6 has the lowest frequency and should therefore be the most efficient donor mode according to computational work, the fraction of C_6F_6 molecules with 2000 cm^{-1} of energy in ν_{16} is smaller than the other donors; therefore, ν_{16} in C_6F_6 would need to be more 3 times more efficient than ν_{16} in the other donors to have the same energy-transfer probability at $\Delta E = 2000$ cm^{-1}. When $\Delta E = 8000$ cm^{-1} is considered, ν_{16} for C_6F_6 would need to be 8 times more efficient than ν_{16} for pyrazine and pyrimidine to have the same energy-transfer probability. Thus, even though low-frequency modes may have larger energy-transfer cross sections, the fraction of molecules with enough energy in low-frequency modes to affect a given energy transfer is smaller than the fraction of molecules with enough energy in the same higher-frequency mode.

A "fractional energy-transfer distribution", $f(E,E')$, model has been reported elsewhere.[10,21,22] This model takes into account both the efficiency with which a donor vibrational mode can impart energy in collisions and the ability of the mode to impart that energy (the fraction of donor molecules with sufficient energy in the mode to transfer a given ΔE). Energy-transfer efficiency is determined from the points where $P(E,E')$ is equal using vibrational mode fractions calculated at the energy where $P(E,E')$ cross using eq 5. Because mode fractions are needed to obtain the efficiency factor, only one vibrational mode can be compared at a time and those modes must have the same molecular motion. Thus it is necessary to assume that energy-

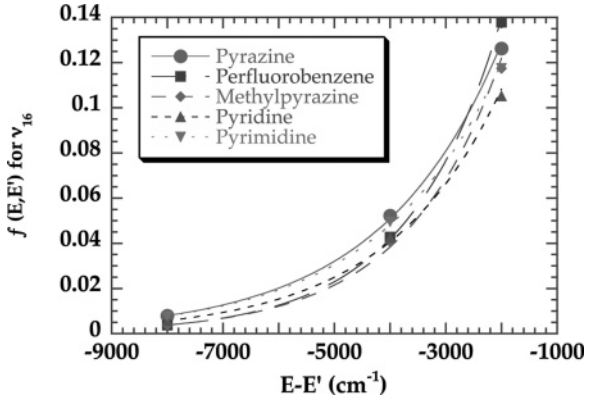

Figure 9. $f(E,E')$ function (fractional mode populations times an efficiency factor) for the ν_{16} out-of-plain mode for pyridine, pyrimidine, pyrazine, methylpyrazine, and C_6F_6 as a function of $\Delta E = E - E'$ (cm^{-1}). $f(E,E')$ is calculated according to a method detailed in refs 10 and 21. The shape of these $f(E,E')$ functions have the same qualitative shape as experimental $P(E,E')$ in Figure 4. Note that functions cross one in the same way as experimental $P(E,E')$.

transfer results entirely from a single mode and an $f(E,E')$ curve is created for each vibrational mode that has a molecular motion common between the donors. The ν_{16} vibrational mode of C_6F_6 must be 3.3 times more efficient than the same pyrazine molecular motion at transferring energy according to this method and 3.1, 2.7, and 2.9 times more efficient than the equivalent pyrimidine, pyridine, and methylpyrazine motion, respectively. Efficiency factors are also determined for other molecular motions common among the donors.

This efficiency factor is then multiplied by the mode populations obtained from eq 5 at various energies (ΔE) to give $f(E,E')$ for that mode. If we assume the energy-transfer events that populate the large ΔE portion of $P(E,E')$ result entirely from energy leaking out of ν_{16}, using the fractional populations from Table 4, we can calculate the fractional energy-transfer distribution functions for pyrazine, pyridine, pyrimidine, methylpyrazine, and C_6F_6 for collisional energy transfers to CO_2 over $\Delta E = 2000-8000$ cm^{-1}. The $f(E,E')$ curves for ν_{16} are shown in Figure 9 and qualitatively match the shape of the experimental $P(E,E')$s shown in Figure 4 in terms of curve crossing and general trends of the curves relative to each other. In fact, the $f(E,E')$ curves created using ν_{16} more closely match the $P(E,E')$ shape and trends than those created using other donor vibrational modes common between all the donor molecules.

In using this model, one must recognize the limitations. First it is only possible to determine relative efficiency of the same molecular motion between different donors; it is not possible to determine the relative efficiency of different modes within the same donor molecule. Second, even though donor mode efficiency is most likely different at different values of ΔE, because the efficiency factor can only be determined at points of equal energy-transfer probability, a constant efficiency factor is used for all ΔE. Finally, one can only consider the effect of vibrational motion common to all donors. Even with these limitations, this model suggests that the lowest-frequency mode for each donor is the principal determiner of the shape of $P(E,E')$, even though energy transfer likely results from energy leaking out of all vibrational modes. The $f(E,E')$ model functions are consistent with the Fermi's Golden Rule model, which indicates that $P(E,E')$ shape is governed by how donor-state densities change which is in turn governed primarily by the low-frequency modes. The $f(E,E')$ model functions are also consistent with the quantum scattering[41] and classical trajectory[39,40] work that implicates low-frequency, particularly out-of-plane modes as the supercollision gateways. The $f(E,E')$ model further clears up the apparent discrepancy between the Fermi's Golden Rule model that suggests that supercollisions are maximized for donors with high-frequency stiff modes and computational studies that indicate supercollisions are maximized by low-frequency floppy modes, because the $f(E,E')$ model considers not only of the efficiency of a given mode at transferring energy but also of the number of molecules in that mode with a sufficient energy to impart ΔE to the bath in a collision. A consistent picture is developing that connects low-frequency donor vibrational motion to the shape of $P(E,E')$, in particular, specific low-frequency modes to supercollisions.

V. Conclusion

The relaxation of highly vibrationally excited pyridine ($E_{vib} = 40\ 660$ cm^{-1}) in collisions with a bath of carbon dioxide has been studied using infrared diode laser spectroscopy to probe scattered bath molecules. The nascent rotational populations and recoil velocity distributions for rotational states in the high-J tail ($J = 58-80$) of the 00^00 level of CO_2 were measured. The recoil velocity distributions indicate that bath molecules scattered into high-J states of the ground vibrational level undergo significant translational and rotational excitation. However, quantum-state-resolved energy-transfer probability data indicate that pyridine/CO_2 energy-transfer events occur less frequently than has been observed in previously studied systems with this amount of internal energy.

State-indexed energy-transfer probabilities have been re-sorted as a function of ΔE to extract the high-energy tail of the energy-transfer distribution function, $P(E,E')$. $P(E,E')$ for pyridine has been compared to $P(E,E')$ for C_6F_6, pyrazine, methylpyrazine, and pyrimidine obtained previously. Although collisions that transfer large amounts of energy are evident for all molecules, the "supercollision" tail behaves differently for each. Double exponential fits to $P(E,E')$ give the following results. The "fraction" of "strong" collisions is found to be $f = 0.03$, the characteristic parameter of "strong" collisions is found to be $\gamma = 1731$ cm^{-1}, and the characteristic parameter of "weak" collisions is found to be $\alpha = 337$ cm^{-1} for pyridine/CO_2 collisions. The shape of the large ΔE tail of $P(E,E')$ for pyridine, as determined by γ, indicates that pyridine is in the middle of the range of strong-collision energy-transfer donors studied to date in terms of magnitude.

Two models have been used to consider the effects of molecular properties on $P(E,E')$. An $f(E,E')$ model, which considers both donor mode efficiency and population, most accurately mirrors the shape of $P(E,E')$ when low-frequency out-of-plane donor modes are assumed to dominate the large ΔE energy-transfer processes, and a model based on Fermi's Golden Rule indicates that the way in which the donor density of states changes with ΔE determines the shape of $P(E,E')$. When considered together, these two models provide a consistent picture indicating that $P(E,E')$ shape is governed by low-frequency donor motion, which are the gateways through which energy leaks out of the donor into the bath.

Acknowledgment. This work was performed at Brigham Young University with support from the BYU Mentoring Environment Grant. J.A.J. acknowledges support from the BYU Office of Research and Creative Works Fellowship program. J.A.J., M.M., and D.G.M. acknowledge support from the Department of Chemistry and Biochemistry Undergraduate Research Awards program.

References and Notes

(1) Lindemann, F. A. *Trans. Faraday Soc.* **1922**, *17*, 598.
(2) Gilbert, R. G.; Smith, S. C. *Theory of Unimolecular and Recombination Reactions*; Blackwell Scientific Publications: Oxford, U.K., 1990.
(3) Michaels, C. A.; Flynn, G. W. *J. Chem. Phys.* **1997**, *106*, 3558.
(4) Hold, U.; Lenzer, T.; Luther, K.; Reihs, K.; Symonds, A. C. *J. Chem. Phys*. **2000**, *112*, 4076.
(5) Liu, C.-L.; Hsu, Hsu, C.; Lyu, J.-J.; Ni, C.-K. *J. Chem. Phys.* **2005**, *123*, 131102.
(6) Flynn, G. W.; Weston, R. E., Jr. *J. Phys. Chem.* **1993**, *97*, 8116.
(7) Mullin, A. S.; Park, J.; Chou, J. Z.; Flynn, G. W.; Weston, R. E., Jr. *Chem. Phys*. **1993**, *175*, 53.
(8) Mullin, A. S.; Michaels, C. A.; Flynn, G. W. *J. Chem. Phys*. **1995**, *102*, 6032.
(9) Michaels, C. A.; Lin, Z.; Mullin, A. S.; Tapalian, H. C.; Flynn, G. W. *J. Chem. Phys.* **1996**, *106*, 7055.
(10) Sevy, E. T.; Rubin, S. M.; Lin, Z.; Flynn, G. W. *J. Chem. Phys.* **2000**, *113*, 4912.
(11) Wall, M. C.; Stewart, B. A.; Mullin, A. S. *J. Chem. Phys.* **1998**, *108*, 6185.
(12) Park, J.; Li, Z.; Lemoff, A. S.; Rossi, C.; Elioff, M. S.; Mullin, A. S. *J. Phys. Chem. A* **2002**, *106*, 3642.
(13) Park, J.; Shum, L.; Lemoff, A. S.; Werner, K.; Mullin, A. S. *J. Chem. Phys.* **2002**, *117*, 5221.
(14) Miller, E. M.; Murat, L.; Bennette, N.; Hayes, M.; Mullin, A. S. *J. Phys. Chem. A* **2006**, *110*, 3266.
(15) Elioff, M. S.; Fang, M.; Mullin, A. S. *J. Chem. Phys.* **2001**, *115*, 6990.
(16) Li, Z.; Korobkova, E.; Werner, K.; Shum, L.; Mullin, A. S. *J. Chem. Phys.* **2005**, *123*, 174306.
(17) Elioff, M. S.; Wall, M. C.; Lemoff, A. S.; Mullin, A. S. *J. Chem. Phys.* **1999**, *110*, 5578.
(18) Wall, M. C.; Lemoff, A. S.; Mullin, A. S. *J. Phys. Chem. A* **1998**, *102*, 9101.
(19) Wall, M. C.; Lemoff, A. S.; Mullin, A. S. *J. Chem. Phys.* **1999**, *111*, 7373.
(20) Wall, M. C.; Mullin, A. S. *J. Chem. Phys.* **1998**, *108*, 9658.
(21) Johnson, J. A.; Duffin, A. M.; Hom, B. J.; Jackson, K. E.; Sevy, E. T. *J. Chem. Phys.* **2008**, *128*, 054304.
(22) Mitchell, D. G.; Johnson, A. M.; Johnson, J. A.; Judd, K. A.; Kim, K.; Mayhew, M.; Powell, A. J.; Sevy, E. T. *J. Phys. Chem. A* **2008**, *112*, 1157.
(23) Duffin, A. M.; Johnson, J. A.; Muyskens, M. A.; Sevy, E. T. *J. Phys. Chem. A* **2007**, *111*, 13330.
(24) Yamazaki, I.; Murao, T.; Yamanaka, T.; Yoshihara, K. *Faraday Discuss. Chem. Soc.* **1983**, *75*, 395.
(25) Bolovinos, A.; Tsekeris, P.; Philis, J.; Pantos, E.; Andritsopoulos, G. *J. Mol. Spectrosc.* **1984**, *103*, 240.
(26) Khan, F. A.; Kreutz, T. G.; Flynn, G. W.; Weston, R. E., Jr. *J. Chem. Phys.* **1990**, *92*, 4876.
(27) Parker, G. A.; Pack, R. T. *J. Chem. Phys.* **1978**, *68*, 1585.
(28) Abrams, R. L.; Cheo, P. K. *Appl. Phys. Lett.* **1969**, *15*, 177.
(29) Agrawal, P. M.; Raff, L. M. *J. Chem. Phys.* **1981**, *75*, 2163.
(30) Brownsword, R. A.; Salh, J. S.; Smith, I. W. M. *J. Chem. Soc., Faraday Trans.* **1995**, *91*, 191.
(31) Pack, R. T. *J. Chem. Phys.* **1979**, *70*, 3424.
(32) Roche, C.; Millot, G.; Chaux, R.; Saint-Loup, R. *J. Chem. Phys.* **1994**, *101*, 2863.
(33) Hershberger, J. F.; Chou, J. Z.; Flynn, G. W.; Weston, R. E., Jr. *Chem. Phys. Lett.* **1988**, *149*, 51.
(34) Havey, D. K.; Liu, Q.; Li, Z.; Elioff, M.; Fang, M.; Neudel, J.; Mullin, A. S. *J. Phys. Chem. A* **2007**, *111*, 2458.
(35) Troe, J. *J. Chem. Phys.* **1992**, *97*, 288.
(36) Troe, J. *J. Chem. Phys.* **1977**, *66*, 4758.
(37) Lendvay, G.; Schatz, G. C.; Harding, L. B. *Faraday Discuss.* **1995**, *102*, 389.
(38) Lin, M.-F.; Dyakov, Y. A.; Tseng, C.-M.; Mebel, A. M.; Lin, S. H.; Lee, Y. T.; Ni, C.- K. *J. Chem. Phys.* **2005**, *123*, 54309.
(39) Lendvay, G. *J. Phys. Chem. A* **1997**, *101*, 9217.
(40) Lendvay, G.; Schatz, G. C. *J. Chem. Phys.* **1992**, *96*, 4356.
(41) Clary, D. C.; Gilbert, R. G.; Bernshtein, V.; Oref, I. *Faraday Discuss.* **1995**, *102*, 423.
(42) Durana, J. F.; McDonald, J. D. *J. Chem. Phys.* **1976**, *64*, 2518.
(43) Smith, I. W. M. *Kinetics and Dynamics of Elementary Gas Reactions*; Butterworths: London, 1980.
(44) Hirschfelder, J. O.; Curtiss, C. F.; Bird, R. B. *Molecular Theory of Gases and Liquids*; John Wiley & Sons, Inc.: New York, 1954.
(45) Lin, H. M.; Seaver, M.; Tang, K. Y.; Knight, A. E. W.; Parmenter, C. S. *J. Chem. Phys.* **1979**, *70*, 5442.
(46) Whitten, G. Z.; Rabinovitch, B. S. *J. Chem. Phys.* **1963**, *38*, 2466.
(47) Sevy, E. T.; Muyskens, M. A.; Lin, Z.; Flynn, G. W. *J. Phys. Chem. A* **2000**, *104*, 10538.
(48) Michaels, C. A.; Tapalian, H. C.; Lin, Z.; Sevy, E. T.; Flynn, G. W. *Faraday Discuss.* **1995**, *102*, 405.
(49) Sevy, E. T.; Michaels, C. A.; Tapalian, H. C.; Flynn, G. W. *J. Chem. Phys.* **2000**, *112*, 5844.
(50) Sevy, E. T.; Muyskens, M. A.; Rubin, S. M.; Flynn, G. W.; Muckerman, J. T. *J. Chem. Phys.* **2000**, *112*, 5829.
(51) Lin, M.-F.; Dyakov, Y. A.; Tseng, C.-M.; Mebel, A. M.; Lin, S. H.; Lee, Y. T.; Ni, C.-K. *J. Chem. Phys.* **2006**, *124*, 84303.
(52) Eaton, V. J.; Steele, D. *J. Mol. Spectrosc* **1973**, *48*, 446.
(53) Pearce, R. A. R.; Steele, D.; Radcliffe, K. *J. Mol. Struct.* **1973**, *15*, 409.
(54) Watanabe, T.; Shimada, H.; Shimada, R. *Bull. Chem. Soc. Jpn.* **1982**, *55*, 2564.
(55) Simmons, J. D.; Innes, K. K. *J. Mol. Spectrosc.* **1964**, *14*, 190.
(56) Billes, F.; Mikosch, H.; Holly, S. *J. Mol. Struct. (THEOCHEM)* **1998**, *423*, 225.
(57) Kline, C. H., Jr.; Turkevich, J. *J. Chem. Phys.* **1944**, *12*, 300.
(58) Martin, J. M. L.; Van, Alsenoy, C. *J. Phys. Chem.* **1996**, *100*, 6973.
(59) Pongor, G.; Pulay, P.; Fogarasi, G.; Boggs, J. E. *J. Am. Chem. Soc.* **1984**, *106*, 2765.